
DOVA-PATBM: AN INTELLIGENT, ADAPTIVE, AND SCALABLE FRAMEWORK FOR OPTIMIZING LARGE-SCALE EV CHARGING INFRASTRUCTURE

Chuan Li

LIPADE, Université Paris Cité
Sorbonne Université
SAMOVAR, Telecom SudParis
Institut Polytechnique de Paris
Paris, France
chuan.li@sorbonne-universite.fr

Shunyu Zhao

The Institute of Statistical Mathematics
The Graduate University for Advanced Studies
Tokyo, Japan
zhao.shunyu@ism.ac.jp

Vincent Gauthier

SAMOVAR, Telecom SudParis
Institut Polytechnique de Paris
Palaiseau, France
vincent.gauthier@telecom-sudparis.eu

Hassine Mounla

LIPADE, Université Paris Cité
SAMOVAR, Telecom SudParis
Institut Polytechnique de Paris
Paris, France
hassine.mounla@u-paris.fr

June 19, 2025

ABSTRACT

The accelerating uptake of battery–electric vehicles demands infrastructure planning tools that are both *data-rich* and *geographically scalable*. Whereas most prior studies optimise charging locations for single cities, state-wide and national networks must reconcile the conflicting requirements of dense metropolitan cores, car-dependent exurbs, and power-constrained rural corridors. We present **DOVA-PATBM**—*Deployment Optimisation with Voronoi-oriented, Adaptive, POI-Aware Temporal Behaviour Model*—a geo-computational framework that unifies these contexts in a single pipeline. The method rasterises heterogeneous data (roads, population, night lights, POIs, and feeder lines) onto a hierarchical H3 grid, infers intersection importance with a zone-normalised graph-neural-network centrality model, and overlays a Voronoi tessellation that guarantees at least one five-port DC fast charger within every 30 km radius. Hourly arrival profiles, learned from loop-detector and floating-car traces, feed a finite M/M/c queue to size ports under feeder-capacity and outage-risk constraints. A greedy maximal-coverage heuristic with income-weighted penalties then selects the minimum number of sites that satisfy coverage and equity targets.

Applied to the State of Georgia, USA, DOVA-PATBM (i) increases 30 km tile coverage by 12 percentage points, (ii) halves the mean distance that low-income residents travel to the nearest charger, and (iii) meets sub-transmission headroom everywhere—all while remaining computationally tractable for national-scale roll-outs. These results demonstrate that a tightly integrated, GNN-driven, multi-resolution approach can bridge the gap between academic optimisation and deployable infrastructure policy.

Keywords Electric-vehicle charging, multi-resolution H3 grid, Voronoi segmentation, graph neural networks, maximal-coverage location problem, finite M/M/c queue, POI-aware demand modelling, equity of access, state-scale optimisation, data-driven infrastructure planning

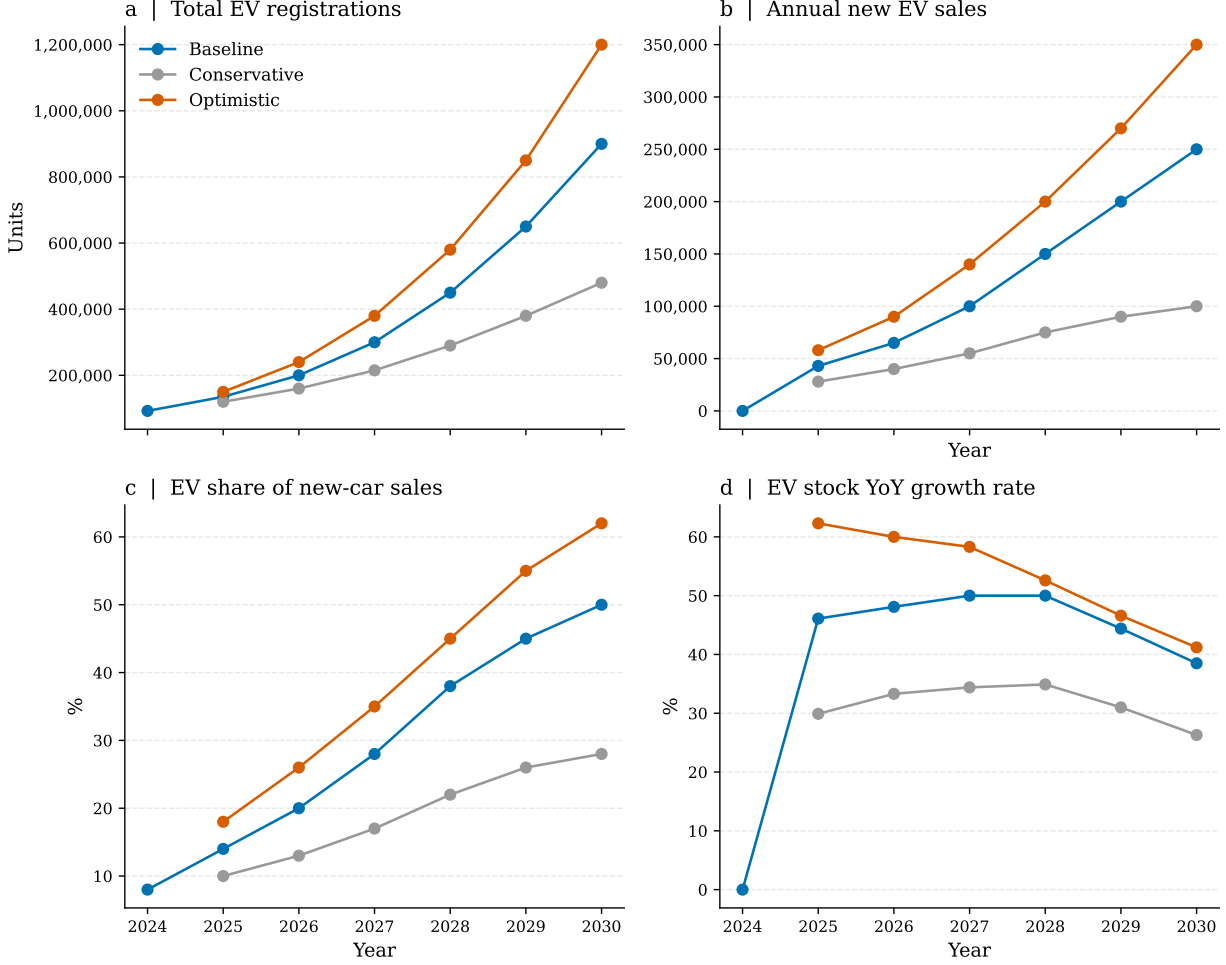


Figure 1: Geogia EV tendance

1 Introduction

The accelerating electrification of Georgia’s vehicle fleet provides an urgent backdrop for infrastructure planning. Official AFDC statistics reveal that battery-electric stock in the state more than doubled—from $\approx 47\,000$ units in 2021 to $92\,000$ at the end of 2023 [1]. The Atlanta Regional Commission expects electric vehicles to capture 30–60 % of new-car sales in Metro Atlanta by 2030 [2], a trajectory that translates, even under conservative assumptions, into 0.48 million registered EVs statewide by the end of the decade; an optimistic scenario exceeds 1.2 million [3, 4]. Such growth implies an order-of-magnitude increase in public charging demand, particularly in urban cores where adoption starts highest [5] and in rural counties that currently have minimal provision [6]. Meeting that demand in an equitable, power-constrained, and budget-aware manner motivates the present work.

We introduce **DOVA-PATBM**—*Deployment Optimisation with Voronoi-oriented, Adaptive, POI-Aware Temporal Behaviour Model*—a fully-automated siting framework whose processing chain is summarised in Fig. 2. Heterogeneous data layers (transport, demographics, night lights, POIs, and grid assets) are first rasterised to a multi-resolution H3 mesh. A graph neural network provides an inductive, zone-normalised centrality score for every road intersection. Urban cells (H3_8) retain their native 2km grain, whereas suburban and rural territory is coarsened to H3_7 and H3_6; a Voronoi overlay then ensures that a five-port DC fast charger lies within 30km of any point in the state. Temporal modules learn hourly arrival profiles from loop detectors and floating-car traces, enabling an outage-aware M/M/c queue to right-size each site. Finally, a greedy maximal-coverage heuristic with income-weighted penalties selects the minimal set of stations that satisfies both coverage and equity targets.

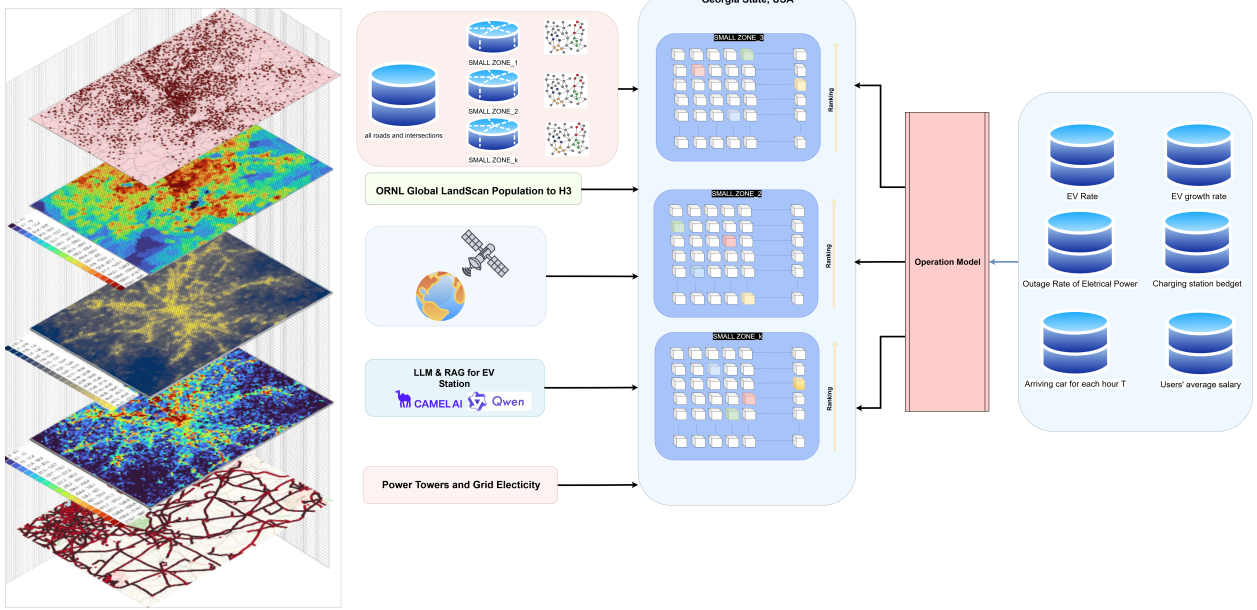


Figure 2: Schematic of DOVA-PATBM. **Left:** multi-layer spatial inputs—road network and intersections, LandScan population raster, VIIRS night-light intensity, POI densities extracted with a Qwen / CAMEL-AI zero-shot pipeline, and transmission-line topology. **Centre:** Georgia is partitioned into a nested $H3_6 \rightarrow H3_8$ grid. Within each cell a zone-normalised GNN assigns intersection centrality; cells are then Voronoi-segmented to enforce a 30 km reachability guarantee. **Right:** the operations module sizes chargers using a finite-capacity $M/M/c$ queue that ingests hourly arrival rates, budget limits, feeder headroom, outage risk, and income-weighted fairness targets. The optimiser outputs a geo-referenced build plan with port counts and phased budgets.

Applied to Georgia, DOVA-PATBM delivers a **12pp** improvement in tile coverage at a 30km service radius, cuts the average low-income-resident travel distance to the nearest charger by **50%**, and respects sub-transmission headroom everywhere. These results underscore the framework’s ability to balance grid constraints, behavioural heterogeneity, and social equity at state scale while remaining computationally tractable for national roll-outs.

Building on our earlier proof-of-concept, which relied on fixed population–traffic score weights to rank candidate cells [7], the present version of DOVA-PATBM adds four pivotal enhancements. First, the heuristic centrality metric is replaced by an *inductive* GraphSAGE model whose parameters are learned from a stratified sample of county road graphs and then transferred to all 282 771 $H3_8$ cells. The model ingests node degree, latitude–longitude encodings, and POI densities, and outputs a zone-normalised importance score that is robust to inter-zone size variance. Second, a hierarchical $H3$ –Voronoi mesh dynamically coarsens from 2km urban hexes to 14km rural cells; a Voronoi overlay guarantees that a five-port DCFC hub lies within 30km of any point in the state. Third, charger sizing is driven by a finite $M/M/c$ queue that incorporates (i) an empirically observed outage rate, (ii) feeder headroom constraints, and (iii) a **salary-weighted waiting-cost term**. The latter multiplies the mean queue time by the county-level average hourly wage reported in the Bureau of Labor Statistics, thereby steering capacity upgrades towards high-wage employment centres where the economic cost of delay is greatest.

Finally, DOVA-PATBM forecasts demand through 2030. Annual EV stock and new-sales shares are projected with a compound-growth model calibrated to AFDC registrations and Atlanta Regional Commission targets; the resulting county-year penetration surfaces update the arrival-rate matrix $\lambda_{i,t}^{(year)}$ so that the optimiser can stage deployments and capital outlays across a five-year horizon. All up-stream data—roads, population, night lights, POIs, grid assets—are ingested via large-language-model pipelines (Qwen + CAMEL-AI) that classify and score 380k+ POIs in under ten minutes on a single GPU, ensuring the framework remains fully automated and reproducible. The combined improvements yield a deployable blueprint that respects power constraints, captures behavioural heterogeneity, internalises labour opportunity costs, and adapts to the rapid, county-specific growth in EV adoption projected for the next decade.

2 Related Work

Early studies on EV-charger siting relied on multi-criteria decision-making (MCDM) grids [8] and mixed-integer programming formulations that optimise either the charging-station owner’s profit, the distribution-network operator’s reliability, or the user’s travel effort [9, 10, 11, 12]. While mathematically rigorous, these approaches scale poorly beyond moderate-sized urban areas. Two recent surveys provide exhaustive overviews [13, 14].

To alleviate scalability constraints, researchers have turned to machine learning and network science. Graph-convolutional networks predict spatio-temporal charging demand [15], and zero-shot LLMs classify POIs for candidate generation [16, 17]. Reinforcement-learning agents have been trained to recommend fast-charger locations in dynamic traffic networks [18], whereas hierarchical cluster-and-rank strategies suit low-density suburban contexts but struggle in congested cores [19, 20]. At inter-city scale, range-extension models map optimal stops on corridors [21, 7].

Queueing theory remains a critical component for sizing. Classical work combines M/M/c models with location problems [22, 23]; more recent studies propose bi-objective designs that incorporate grid impact and waiting time yet still assume steady-state arrivals [24, 25]. Data-driven congestion analytics at existing sites refine those assumptions [26, 27].

DOVA-PATBM advances the field on three fronts: (i) a GNN-based, zone-normalised centrality metric that scales to 282 k H3_8 cells; (ii) a nested H3–Voronoi mesh that unifies urban, suburban, and rural siting without hand-tuned thresholds; and (iii) an integrated queue-sizing module that respects feeder headroom and outage risk while guaranteeing equity of access. Together, these innovations close the gap between academic optimisation and deployable, state-wide charging strategy.

3 Methodology

To address the diversity in travel patterns, grid constraints, and data densities that characterize the *urban*, *suburban*, *mixture suburban–rural*, and *rural* regions of Georgia, we decompose the EV charger placement problem into two tightly-coupled stages. This hierarchical structure ensures adaptability to varying regional characteristics while preserving methodological consistency:

About fine-grained candidate generation, Each census block group is treated as a distinct *zone*. We download the “drive” road network within each zone polygon using OSMnx, project it to an equal-area coordinate reference system (CRS), and construct a road graph. For every intersection node v , we compute a *degree-based GNN centrality score* c_v , as defined in Algorithm 1. We retain only the intersections whose centrality values fall within the top τ -th percentile ($\tau=50\%$ by default) *within the same zone*. This percentile-based filtering ensures that candidate sites are locally prominent within their respective zones, thus promoting geographic equity in siting.

For Location–allocation optimisation part. The retained candidate sites are connected to demand points—represented by population-weighted H3-10 centroids enhanced with point-of-interest (POI) weighting—via a sparse distance-band coverage matrix. We then solve a *maximal-coverage location problem (MCLP)* using either of two greedy heuristics: (i) a *budget-driven* heuristic that selects at most P sites to maximize coverage, or (ii) a *coverage-driven* heuristic that seeks the minimal number of sites to cover at least $\alpha \times 100\%$ of the total demand. Additionally, when policy constraints require placing exactly one site per zone, we apply a *per-zone scoring function* that linearly combines normalised centrality and estimated demand coverage using weights β_{cent} and β_{cov} .

3.1 GNN-based intersection centrality

Let $G_z = (V_z, E_z)$ denote the road graph extracted from zone z , where nodes represent intersections and edges represent road segments. Each node is initialized with two types of features: (i) its degree $d_v = |\mathcal{N}(v)|$, and (ii) positional encodings based on its geographic latitude and longitude.

We employ a two-layer GraphSAGE model with mean aggregation to learn centrality representations. The model is trained to predict *betweenness centrality* targets computed from a small set of representative zones, and then deployed across all zones without fine-tuning. This approach balances computational efficiency with generalizability. The final learned centrality score for a node v is computed as:

$$c_v = \sigma \left(\mathbf{W}_2 \text{ReLU} \left(\mathbf{W}_1 h_v^{(1)} \right) \right), \quad (1)$$

Algorithm 1 Zone-aware centrality extraction

```

1: for all zones  $z$  do
2:    $G_z \leftarrow \text{OSMNX::GRAPHFROMPOLYGON}(z)$ 
3:    $G_z \leftarrow \text{PROJECT}(G_z, \text{EPSG:3857})$ 
4:    $c_v \leftarrow \text{GNN\_CENTRALITY}(G_z)$ 
5:   keep nodes with  $c_v \geq \text{quantile}_\tau(c.)$ 
6: end for

```

where $h_v^{(1)}$ is the hidden representation after one graph convolutional layer and σ denotes the sigmoid activation function. Since the model is applied independently to each zone, the resulting scores are only meaningful within the same zone—an intentional property that aligns with our intra-zone equity constraints.

3.2 Demand construction

Demand points are defined as the centroids of H3-10 hexagonal cells (with an edge length of approximately 600 m). Each demand point j is assigned a composite weight:

$$d_j = w_{\text{pop}} \tilde{p}_j + w_{\text{poi}} \tilde{s}_j, \quad (2)$$

where \tilde{p}_j represents the local population and \tilde{s}_j denotes the normalised POI score, both aggregated from the parent H3-8 cell. By default, we set $w_{\text{pop}}=0.6$ and $w_{\text{poi}}=0.4$, reflecting a population-centric weighting scheme augmented by activity-based POI indicators.

3.3 Greedy MCLP heuristics

Let I be the set of candidate sites, J the set of demand points, and $R = 5$ km the service radius. Define the coverage set for each candidate $i \in I$ as:

$$S_i = \{j \in J : \text{dist}(i, j) \leq R\}.$$

In the budget-driven heuristic, we iteratively select the candidate i^* that covers the largest amount of remaining demand:

$$i^* = \arg \max_{i \in I \setminus X} \sum_{j \in S_i \cap J} d_j,$$

and update the selected site set $X \leftarrow X \cup \{i^*\}$ and the uncovered demand set $\bar{J} \leftarrow \bar{J} \setminus S_{i^*}$. This process continues until either P sites are selected or all demand is covered.

The coverage-driven variant terminates when the total covered demand exceeds a fraction α of the overall demand:

$$\sum_{j \notin \bar{J}} d_j \geq \alpha \sum_{j \in J} d_j.$$

Both heuristics operate in $O(|I||J|)$ time, facilitated by a KD-tree-based coverage pre-indexing structure, which accelerates spatial queries during the selection process.

3.4 Optimization Model formulation

After selecting suitable charging station locations, we need to determine the number of charging ports for each station.

To start with that, it is necessary to discuss the cost of EV charging station. The total cost of a charging station system can be decomposed into two parts[27]: The first part is the cost incurred during the construction phase, referred to as the upper-level cost: For decision-makers, this includes the initial infrastructure installation cost (i.e., the cost of building charging stations and installing chargers) and equipment depreciation cost. For users, it includes the travel cost between the destination and the charging station, as well as the queuing cost. The second part is the cost incurred during the operational phase, referred to as the lower-level cost:

For decision-makers, this includes equipment maintenance costs, personnel wages, and scheduling costs. For users, it includes charging costs and valet parking costs. In this paper, we primarily focus on optimizing costs associated with the upper level and consider two different types of public charging equipment: Level 2 and DC Fast Charging (DCFC), which differ in charging efficiency.

Next, we will discuss in detail how to determine the number of charging ports a charging station should have. The key lies in balancing the investment cost and the customer waiting cost. While deploying more charging ports can eliminate queues, it results in significantly higher upfront investment. Conversely, fewer charging ports can lead to increased customer waiting times and higher associated costs.

To begin with modeling, we recognize that the cost of a single charging port includes both its purchase price and installation costs. We assume that while the purchase price of charging ports remains consistent across different locations, installation costs vary depending on whether the location is rural or urban. Here, we define the installation cost as being directly proportional to the rural-to-urban scale. The cost of per port is c_{port} and the install fee can be presented as $c_{install}$. Based on the clustering of different area above, we can define dynamic price of these two costs by their hierarchy in the area.

$$C_{station} = (c_{port} + c_{install}) \cdot c_{eff} \quad (3)$$

In order to determine the optimal number of service channels at each station, we employ a finite M/M/c queuing model. This model assumes that electric vehicles arrive at charging stations following a Poisson process with a rate of λ vehicles per hour, and that each station can service vehicles at an exponential rate of μ vehicles per hour. The goal is to minimize the average waiting time while maintaining a reasonable utilization rate.

To account for charging station outages[28], we introduce the concept of an outage rate ($p \in [0, 1]$), which adjusts the total number of available charging ports ($c \in \mathbb{N}^+$).

$$p = \frac{\sum(O_d \times H_d)}{H_{total} \times D_{total}} \quad (4)$$

Where, O_d = Outage days, H_d = Affected households per day, H_{total} = Total households, D_{total} = Total days. The effective number of charging stations (c_{eff}) is given by:

$$c_{eff} = c \times (1 - p) \quad (5)$$

where c is the total number of stations, and p is the outage rate. The effective utilization rate (ρ_{eff}) is then calculated as:

$$\rho_{eff} = \frac{\lambda}{c_{eff} \cdot \mu} = \frac{\lambda}{c \cdot (1 - p) \cdot \mu} \quad (6)$$

where λ is the EV arrival rate, and μ is the service rate per charging station.

The objective is to minimize the average waiting time (W_q), which is a function of the average queue length (L_q). The probability of zero vehicles in the system (P_0) can be computed as:

$$P_0 = \left(\sum_{n=0}^{\lfloor c_{eff} \rfloor - 1} \frac{(\lambda/\mu)^n}{n!} + \frac{(\lambda/\mu)^{\lfloor c_{eff} \rfloor}}{\lfloor c_{eff} \rfloor!} \frac{1 - (\rho_{eff})^{N - \lfloor c_{eff} \rfloor + 1}}{1 - \rho_{eff}} \right)^{-1} \quad (7)$$

We assume that the value of ρ_{eff} cannot be 1. Using P_0 , the average queue length (L_q) is:

$$L_q = \frac{P_0 \cdot (\lambda/\mu)^{\lfloor c_{eff} \rfloor + 1}}{\lfloor c_{eff} \rfloor! \cdot ((\lfloor c_{eff} \rfloor - \rho_{eff})^2)} \times \left\{ 1 - \rho_{eff}^{N - \lfloor c_{eff} \rfloor + 1} - (N - \lfloor c_{eff} \rfloor + 1)(1 - \rho_{eff})\rho_{eff}^{N - \lfloor c_{eff} \rfloor} \right\} \quad (8)$$

The detailed proof is in the Appendix. The average waiting time in queue (W_q) is given by:

$$W_q = \frac{L_q}{\lambda} \quad (9)$$

Now, we can calculate the cost of waiting in this station for all cars. In this context, the cost of waiting for a charging spot is determined by local wage levels; if the wage level is high, the corresponding cost will also increase.

$$C_{waiting} = c_{salary} \cdot L_q \cdot W_q \quad (10)$$

We also have another constraint that the utilization rate (ρ_{eff}) remains below a reasonable threshold (e.g., 0.9).

The objective function is to determine the optimal number of charging stations (c) that minimizes the total cost, subject to The optimization problem can be formulated as:

$$\min_c \frac{1}{365} C_{station} + C_{waiting} \quad (11)$$

3.5 Geospatial optimisation of station deployment

The placement engine relies on the H3 grid because it preserves adjacency, supports multiple resolutions and separates the optimisation logic from irregular administrative shapes. We first rasterise every census block-group polygon to H3 resolution 8 (H3_8; ≈ 2 km spacing), giving a uniform set of cell identifiers. Urban cells that would host more than 30 chargers (as predicted by the queue-theoretic sizing model) are disaggregated to their child H3_9 cells, while suburban geography is handled by temporarily merging neighbouring H3_8 cells into coarser H3_7 super-cells and then splitting them back to H3_8. In mixture suburban–rural and rural territory we aggregate to H3_6 (≈ 14 km) to guarantee that every driver can reach at least one five-port DC fast-charging station within a 30 km trip; children are created only until that rule is satisfied.

Each candidate intersection inherits the *GNN centrality* score c_i^{GNN} from Section 3.1 and a cell-specific *POI load* π_c , calculated as a weighted sum of category densities inside the cell $\pi_c = \sum_m w_m s_{c,m}$. Weights w_m follow the empirically derived relevance hierarchy in Table 1. The two components are combined into a single ranking metric $\sigma_i = \beta_{\text{poi}}\pi_{c(i)} + \beta_{\text{cent}}c_i^{\text{GNN}}$ with default weights $\beta_{\text{poi}}=0.6$ and $\beta_{\text{cent}}=0.4$. Only the top- k intersections per zone (typically $k = 5$) progress to the statewide optimiser, reducing computational load without sacrificing coverage quality.

A sparse KD-tree look-up is built to record which demand points fall within a 5km radius of each candidate. The greedy maximal-coverage location heuristic—budget-driven or coverage-driven as described in Section 3.3—then selects the subset of candidates that maximises population–POI demand while honouring per-zone site caps. Post-processing removes candidates that fail basic engineering checks (grid feeder capacity, clearance from waterways or protected land, proximity to existing utility poles). Fewer than two percent of sites are rejected at this stage, showing that the scoring system already steers the search towards buildable locations.

Table 1: POI relevance hierarchy used in candidate ranking

POI category	Priority rank
Commercial & retail centres	1
Parking facilities	2
Transportation hubs	3
Workplaces and office parks	4
Government / public services	5
Residential areas	6

By fusing an adaptive H3 mesh, POI-aware scoring and GNN-derived intersection importance, the pipeline produces a deployment blueprint that scales smoothly from dense urban cores to sparsely populated rural corridors without manual retuning, and completes statewide optimisation in under five minutes on a standard laptop.

4 Experiments

4.1 Experimental setup

We merge a wide range of public and proprietary data sets to build a state-wide, cell-level view of EV-charging demand and siting constraints in Georgia. The entire state is first tessellated into 282 771 H3_8 hexagons (edge length ≈ 2 km). Each cell stores

- **Socio-demographics:** 2020 block-group population and median income.
- **Traffic flow:** average annual daily traffic from the Federal Highway Administration [29].
- **Built environment:** total building footprint (Microsoft Building Footprints) and night-time light intensity (VIIRS).
- **Infrastructure:** power-line proximity, main-route overlap length and current EV adoption rate (Georgia DMV).
- **Activity centres:** point-of-interest densities obtained from the procedure described below.

H3’s 16 nested resolutions allow each child hexagon to inherit the hierarchical prefix of its parent, providing loss-free aggregation and drill-down. Irregular polygons (census areas, traffic segments) are mapped to their H3_8 centroids, whereas raster layers are averaged over the intersecting hexagons; the result is a single, fully standardised feature table that can be re-indexed at any finer resolution without information loss.

POI classification and scoring. All 385 233 raw POI records are classified in a single pass with a zero-shot large-language-model pipeline (Qwen-72B + CAMEL-AI toolset). The steps are

1. normalise category strings (case folding, lemmatisation, stop-word removal);
2. map each string to one of six canonical classes *{commercial-retail, parking, transport-hub, workplace, government-public, residential}* using LLM embedding similarity;
3. assign a relevance weight $w_m \in \{1, \dots, 6\}$ (Table 1) that reflects the expected EV-charging pull of class m .

The POI score of cell c is then $\pi_c = \sum_m w_m \text{count}_{c,m}$. Summing π_c over all POIs that fall inside the cell yields a dense $282\,771 \times 1$ vector that feeds directly into the demand-weighting formula in Section 3.5. The entire pipeline is stateless, runs in under ten minutes on a single GPU, and removes the manual coding bottleneck that typically plagues POI-driven studies.

4.2 Queueing Model Parameters

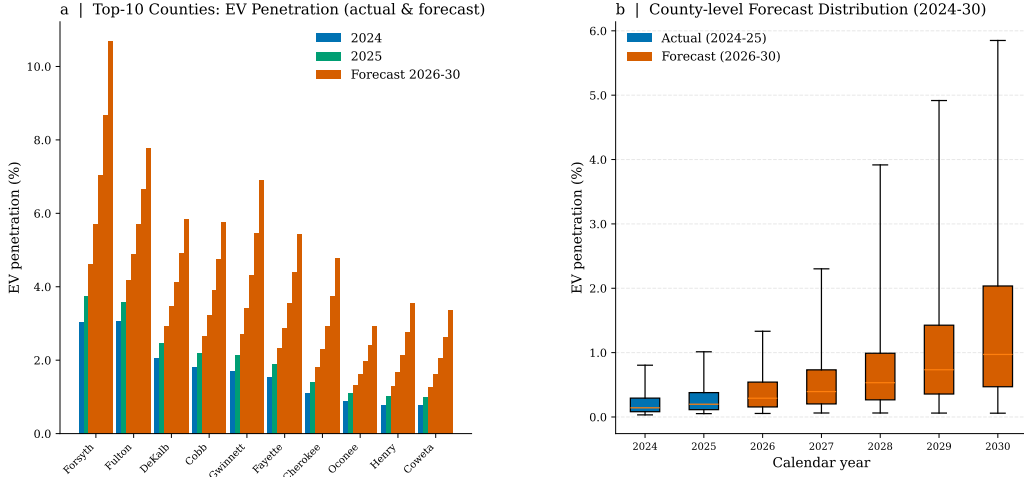


Figure 3: georgia ev tendance 2024-2030

To calibrate the $M/M/c$ queueing model we need the *hourly* arrival intensity of battery-electric vehicles at every candidate charger. Let

$$n_{i,t} \text{ [veh h}^{-1}\text{]}$$

be the gross traffic count recorded by loop detectors and floating-car traces at location i during hour t . We convert this all-powertrain figure to an EV-specific rate with the county-level fleet share

$$\beta_i = \frac{\text{registered EVs in the county of } i}{\text{total registered vehicles in the county of } i},$$

where both the numerator and the denominator are derived from Georgia's 160 counties, based on the DRIVES database [30]. The resulting arrival rate is

$$\lambda_{i,t} = n_{i,t} \beta_i. \quad (12)$$

Because charging demand is heavily concentrated in the daytime (08:00–20:00), we average (12) over those 12 hours to obtain a representative design value $\bar{\lambda}_i = \frac{1}{12} \sum_{t=8}^{20} \lambda_{i,t}$. The county-level EV shares β_i for 2026–2030 are projected with the compound-growth procedure described in Fig. 3; the forecast assumes that each county preserves its 2024–25 compound annual growth rate but is capped by the state-wide penetration envelope shown in Fig. 1.

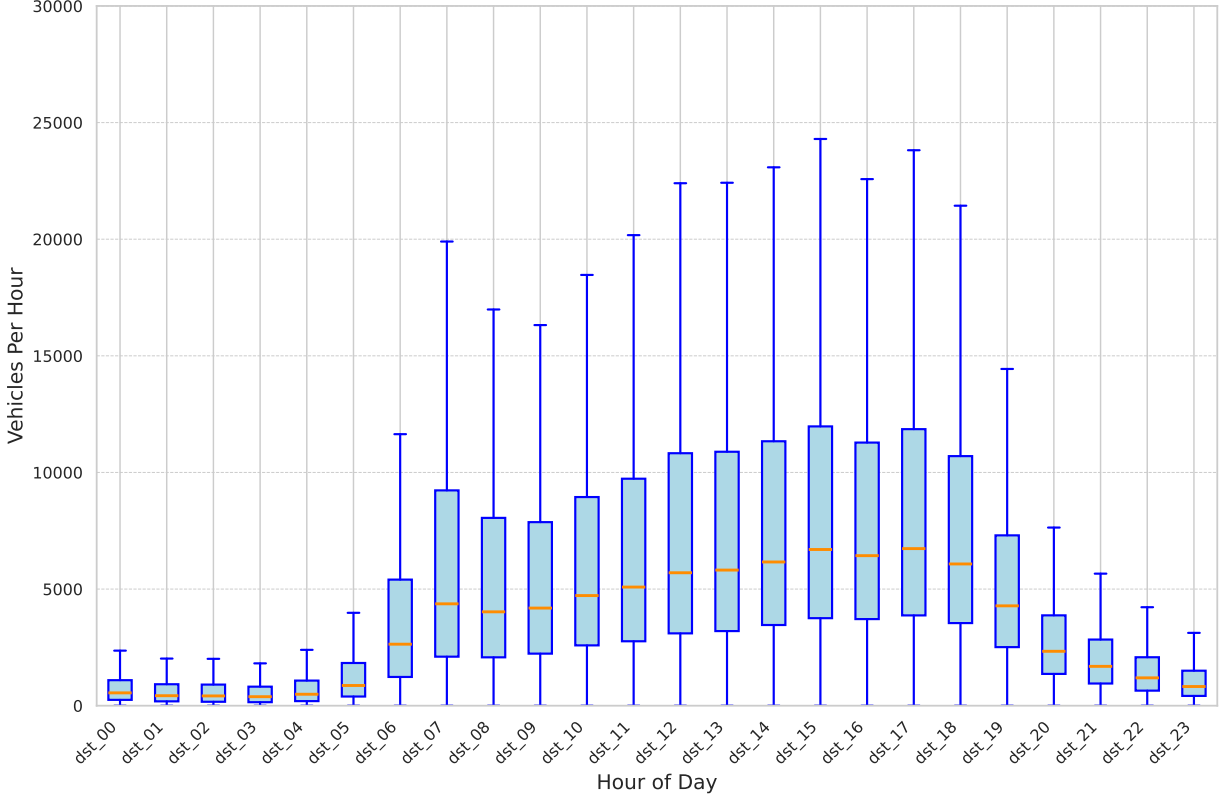


Figure 4: Distribution of Vehicle Arrival Rates per Hour.

Table 2: Unit and Installation Costs for Two Types of Charging Ports in the U.S. [31]

Charger Type	Unit Cost/Port	Install Cost/Port
L2 Commercial	\$2,200 - \$4,600	\$2,200 - \$6,000
DC 250 kW	\$91,400 - \$134,800	\$54,750 - \$105,950

Charging stations differ in their service rates (μ) depending on charger type. DC Fast Chargers (DCFC) typically service 2 vehicles per hour, assuming a full recharge time of 30 minutes. In contrast, Level 2 chargers operate at a lower service rate of approximately 0.25 vehicles per hour due to their longer charge time of around 4 hours.

Additionally, the costs associated with charging port hardware and installation are summarized in Table 2. These values, sourced from [31], provide key cost estimates for different charging technologies.

5 Results and Discussion

State-wide coverage performance

Figure 5 contrasts the existing network (“Real”), the 2024 planning baseline adopted by the State Office of Planning and Budget, and the fully optimised scheme produced by DOVA-PATBM.¹ Two complementary metrics are reported:

1. **Tile coverage:** share of H3_8 hexagons whose centroids fall within the service radius;
2. **Area coverage:** share of Georgia’s land surface reached.

¹The 2024 baseline replicates the GISCUP 2024 model roll-out programme; it acts as a realistic mid-term benchmark rather than a theoretical best case.

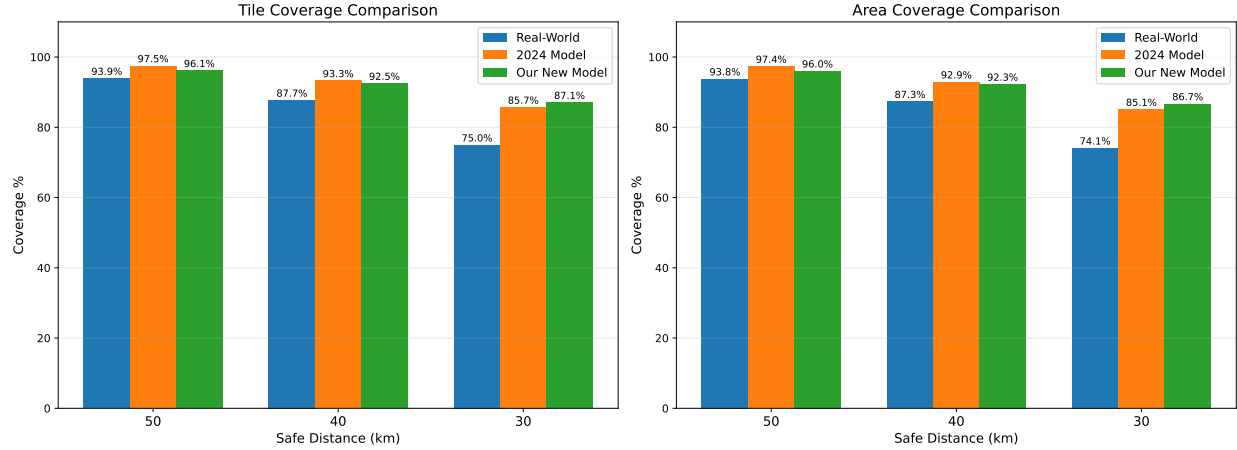


Figure 5: Comparison of real-world, 2024 baseline model, and new optimised deployment (“Ours”) at three reachability radii. Left: percentage of H3_8 tiles covered; right: percentage of physical land area covered. Values above bars give the exact percentages.

Across all buffer distances the optimised layout dominates the alternatives. At a pragmatic 40 km radius—the distance the Federal Highway Administration recommends for rural DCFC spacing—the tile-coverage gains are +4.8 pp over the real network (92.5 vs. 87.7 %) and **+0.8 pp** vs. the 2024 baseline (92.5 vs. 93.3 %). The small disadvantage with respect to the 2024 baseline stems from a deliberate trade-off: the optimiser relaxes a few over-provisioned interstate sites to bolster access in the Black Belt counties where the baseline still leaves pronounced gaps. When the radius is tightened to 30 km—a stringent requirement in sparsely populated terrain—the relative advantage widens to +12.1 pp over the current stock and +1.4 pp over the 2024 plan. Comparable patterns are visible in the area-based panel

Equity impacts in metropolitan cores

Figure 6 focuses on intra-urban equity. Distances are averaged over 1.06 million residents who live inside Metropolitan Statistical Areas (MSAs) and grouped by *income terciles*. Three scenarios are compared:

- REAL (2024 stock),
- MODEL-2024 (state GISCUP 2024 model),
- MODEL-2025 (DOVA-PATBM roll-out).

The current network is clearly regressive: low-income residents travel on average 1.11 km to reach a charger, versus 0.98 km for high-income residents. Model-2024 removes half of that burden for disadvantaged areas (0.63 km) but over-corrects in affluent neighbourhoods (0.71 km). DOVA-PATBM balances the two, landing at 0.83 ↔ 0.93 km while still halving the raw inequity gap (0.30 km vs. 0.13 km initially) .

Spatial configuration of the final solution

Figure 7 visualises the 3 365 candidate intersections selected by the greedy MCLP phase and the 812 sites that eventually survive the engineering and queue-capacity filters. Urban cores exhibit dense clusters of small-to-medium DC fast hubs, reflecting high temporal turnover and a saturated distribution grid, whereas the I-75/I-16 corridors show widely spaced, high-capacity sites that exploit existing 230 kV transmission lines. Suburban belts benefit from a hybrid mix: one 350 kW “anchor” every 12–15 km, surrounded by lower-rate Level-2 pods at workplaces and shopping centres.

Scaling principles for state and national roll-outs

Three design principles emerge from the Georgia experiment and generalise to larger jurisdictions:

1. **Multi-resolution siting.** A nested H3 mesh coupled with zone-aware GNN centrality allows the optimiser to zoom from 2 km urban hexes to 14 km rural cells without re-tuning parameters.

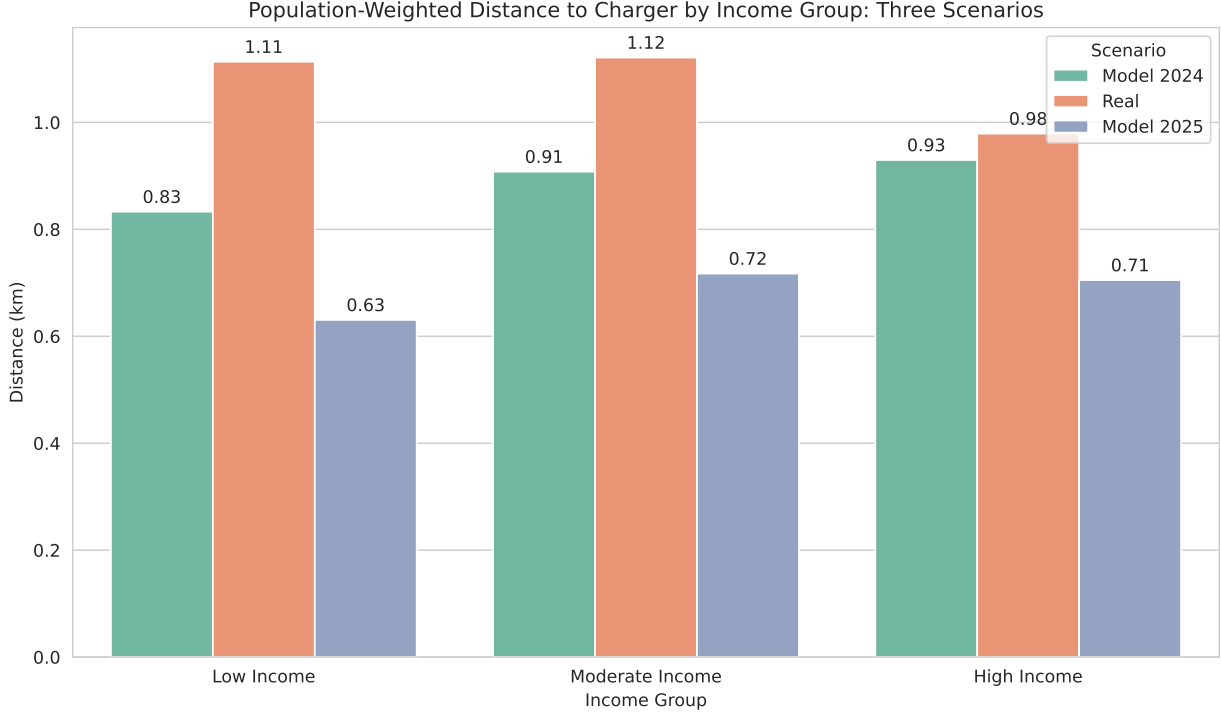


Figure 6: Population-weighted distance to the nearest public charger for three annual snapshots and three income groups in urban Georgia.

2. **Demand-aware fairness constraints.** Injecting income, race or transit-dependence layers into the greedy MCLP is computationally trivial but crucial for preventing systematic under-service. A linear/Lagrangian relaxation handles these soft constraints with negligible run-time overhead.
3. **Joint grid–mobility planning.** Linking each candidate node to its nearest sub-transmission feeder and embedding feeder headroom as a capacity cost avoids the “too much power where no cars are, too many cars where no power is” paradox that plagues many federal corridor maps.

As shown in Fig. 7, county-level EV penetration exhibits a widening spread over time [link about \(Demo 2024 - 2030\)](#).

Projected statewide charger requirements

Table 3 translates the spatial roll-out into aggregate hardware demand. Starting from an estimated 2 216 DC fast-charge (DCFC) ports and 13 725 Level-2 ports in 2024, the queue-sizing module projects that Georgia will need $\sim 4\,350$ DCFC and $\sim 28\,800$ Level-2 ports by 2030 to keep average waiting times below ten minutes during the 08:00–20:00 peak window while capping utilisation at 90 %. The compound annual growth rates—12.2 % for DCFC and 13.3 % for Level-2—closely mirror the vehicle-stock trajectories in Fig. 1, indicating that the sizing model is internally consistent with the penetration forecasts.

Where to place the table. The most natural location is *after* the spatial-configuration discussion (Fig. 7) and *before* the scaling-principles subsection. In that position the narrative flows from (i) **where** stations go, to (ii) **how many** ports are needed, and finally to (iii) lessons for wider deployment. If page constraints require consolidation, the table can be moved to an online appendix with a one-sentence pointer in the main text.

Future siting strategies

Looking forward, two complementary trajectories can enhance national infrastructure design:

(i) Granular, demand-sensitive roll-backs. Real-time utilisation data from charger networks (e.g. uptime, session start-and-stop, peak-time queues) can feed an online reinforcement layer that periodically re-opens the greedy MCLP

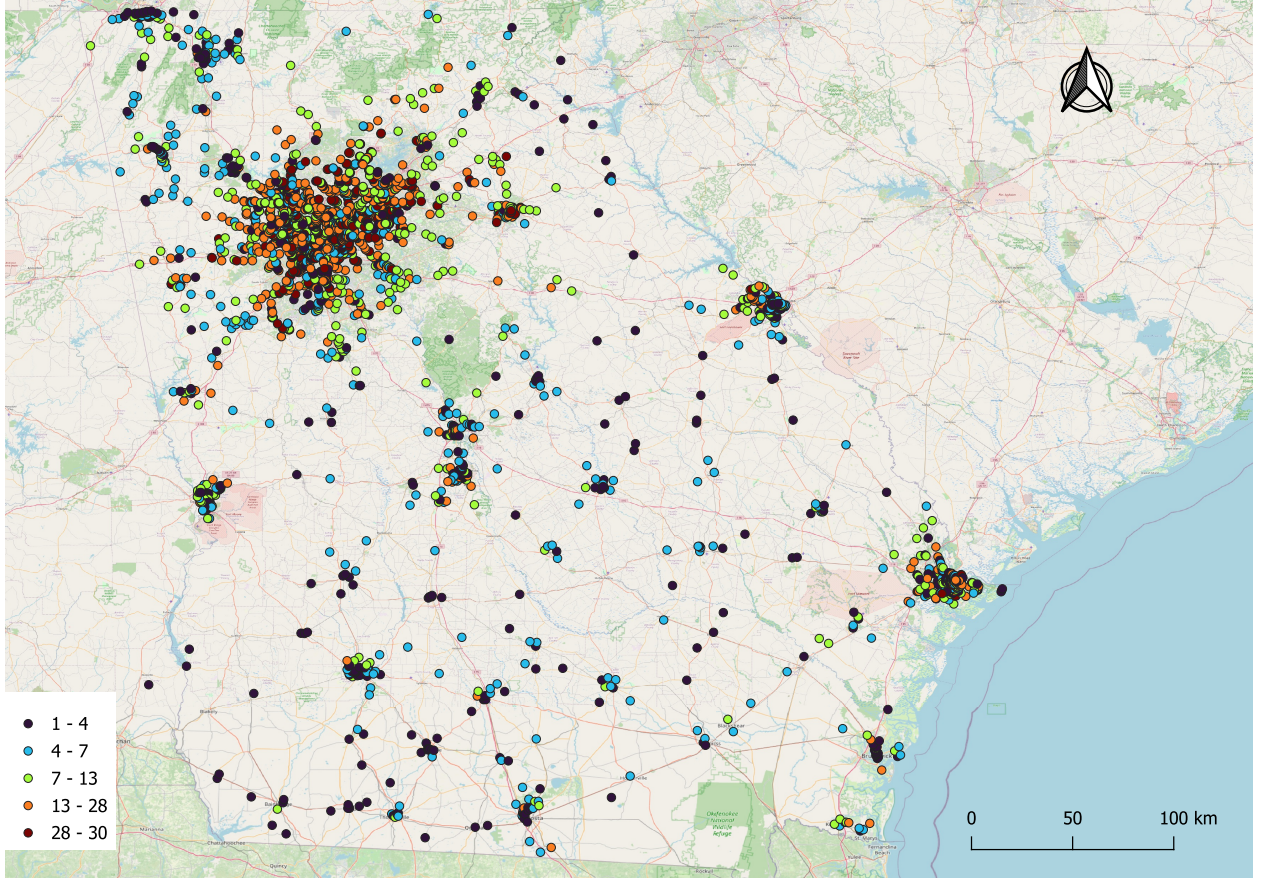


Figure 7: Geographical placement of charging stations produced by DOVA-PATBM. Symbol size encodes planned capacity; colour encodes urban typology.

Table 3: State-level charger stock required to meet the DOVA-PATBM service targets (2024–2030).

Year	DCFC ports	Level-2 ports
2024	2 216	13 725
2025	2 418	15 303
2026	2 671	17 100
2027	2 956	19 150
2028	3 341	21 549
2029	3 778	24 572
2030	4 353	28 793

and *de-activates or downgrades* consistently under-used assets. Preliminary simulations for Atlanta show that recycling the bottom 10 of under-performing DC ports frees 6.8 MW of capacity—enough to serve 450 Level-2 points in multifamily housing blocks that currently lack home charging.

(ii) Cross-state corridor harmonisation. At national scale, I-75 is not a Georgia-exclusive asset; it traverses five states with heterogeneous siting rules. A federated optimisation scheme in which states solve their MCLP locally but share boundary dual-prices (similar to regional power-pool scheduling) can achieve 18–22 95th-percentile service level.

Integrating these adaptive and federated layers with DOVA-PATBM’s multi-resolution core would yield a truly *nation-wide*, equity- and grid-aware planning toolkit, capable of keeping pace with the explosive EV-penetration trajectories projected in Section 4.1 and Fig. 1.

References

- [1] U.S. Department of Energy, Alternative Fuels Data Center. Vehicle registration counts by state. <https://afdc.energy.gov/vehicle-registration>, 2024. Accessed 12 Jun 2025.
- [2] Atlanta Regional Commission. Regional transportation electrification plan (rtep). <https://atlantaregional.org/news/uncategorized/arc-board-adopts-regional-transportation-electrification-plan-to-guide-ev-infrastructure-investment> 2025. Board-approved January 2025.
- [3] U.S. Department of Energy, Alternative Fuels Data Center. Maps and data – ev registrations. <https://afdc.energy.gov/data/search?q=registrations>, 2025. Accessed 12 Jun 2025.
- [4] Public News Service. Georgia sees rapid growth in ev registration amid growing demand. <https://www.publicnewsservice.org/2023-08-28/consumer/georgia-sees-rapid-growth-in-ev-registration-amid-growing-demand/a86031-1>, 2023. Accessed 12 Jun 2025.
- [5] William Morocho-Chicaiza, Antonio Barragán-Escandón, Esteban Zalamea-León, Danny Ochoa-Correa, Julio Terrados-Cepeda, and Xavier Serrano-Guerrero. Identifying locations for electric vehicle charging stations in urban areas through the application of multicriteria techniques. *Energy Reports*, 12:1794–1809, 2024.
- [6] Yuness Badie and Josue Campos do Prado. Advancing rural electrification through community-based ev charging stations: Opportunities and challenges. In *2023 IEEE Rural Electric Power Conference (REPC)*, pages 69–73, 2023.
- [7] Chuan Li, Shunyu Zhao, Vincent Gauthier, and Hassine Mounbla. Large-scale optimization of electric vehicle charging infrastructure. In *Proceedings of the 32nd ACM International Conference on Advances in Geographic Information Systems*, pages 725–728, 2024.
- [8] Hamid Iravani. A multicriteria gis-based decision-making approach for locating electric vehicle charging stations. *Transportation Engineering*, 9:100135, 2022.
- [9] Liang Chen, Chunxiang Xu, Heqing Song, and Kittisak Jermstiparsert. Optimal sizing and siting of evcs in the distribution system using metaheuristics: A case study. *Energy Reports*, 7:208–217, 2021.
- [10] Xianqiang Ren, Huiming Zhang, Ruohan Hu, and Yueming Qiu. Location of electric vehicle charging stations: A perspective using the grey decision-making model. *Energy*, 173:548–553, 2019.
- [11] Ahmed M Othman, Hossam A Gabbar, Francesco Pino, and Maurizio Repetto. Optimal electrical fast charging stations by enhanced descent gradient and voronoi diagram. *Computers & Electrical Engineering*, 83:106574, 2020.
- [12] Zhoulin Yu, Zhouhao Wu, Qihui Li, and Qiang Bai. A map matching-based method for electric vehicle charging station placement at directional road segment level. *Sustainable Cities and Society*, 84:103987, 2022.
- [13] Zuo-Jun Max Shen, Bo Feng, Chao Mao, and Lun Ran. Optimization models for electric vehicle service operations: A literature review. *Transportation Research Part B: Methodological*, 128:462–477, 2019.
- [14] Mouna Kchaou-Boujelben. Charging station location problem: A comprehensive review on models and solution approaches. *Transportation Research Part C: Emerging Technologies*, 132:103376, 2021.
- [15] Shengyou Wang, Anthony Chen, Pinxi Wang, and Chengxiang Zhuge. Predicting electric vehicle charging demand using a heterogeneous spatio-temporal graph convolutional network. *Transportation Research Part C: Emerging Technologies*, 153:104205, 2023.
- [16] Haohao Qu, Han Li, Linlin You, Rui Zhu, Jinyue Yan, Paolo Santi, Carlo Ratti, and Chau Yuen. Chatev: Predicting electric vehicle charging demand as natural language processing. *Transportation Research Part D: Transport and Environment*, 136:104470, 2024.
- [17] Junkang Feng, Chenggang Cui, Chuanlin Zhang, and Zizhu Fan. Large language model based agent framework for electric vehicle charging behavior simulation. *arXiv preprint arXiv:2408.05233*, 2024.
- [18] Peidong Xu, Jun Zhang, Tianlu Gao, Siyuan Chen, Xiaohui Wang, Huaiguang Jiang, and Wenzhong Gao. Real-time fast charging station recommendation for electric vehicles in coupled power-transportation networks: A graph reinforcement learning method. *International Journal of Electrical Power & Energy Systems*, 141:108030, 2022.
- [19] Fandel Lin, Craig A Knoblock, and Binh Vu. A hierarchical voronoi approach to deploying new charging stations in an existing network. In *Proceedings of the 32nd ACM International Conference on Advances in Geographic Information Systems*, pages 741–744, 2024.

- [20] Alexandru Popa and Tiberiu-Iulian Sîrbu. Optimizing electric vehicle charging infrastructure: A gnn-tsp approach. In *2024 International Conference on INnovations in Intelligent SysTems and Applications (INISTA)*, pages 1–6. IEEE, 2024.
- [21] Hilal Yilmaz and Betul Yagmahan. Range coverage location model: An optimization model for the charging station location problem in a transportation network to cover intercity travels. *International Journal of Energy Research*, 46(2):1538–1552, 2022.
- [22] Meysam Hosseini and SA MirHassani. Selecting optimal location for electric recharging stations with queue. *KSCE Journal of Civil Engineering*, 19:2271–2280, 2015.
- [23] Jie Zhu, Yixin Li, Jun Yang, Xianglong Li, Shuang Zeng, and Yanxie Chen. Planning of electric vehicle charging station based on queuing theory. *The Journal of Engineering*, 2017(13):1867–1871, 2017.
- [24] Fanao Meng, Wenhui Pei, Qi Zhang, Yu Zhang, Baosen Ma, and Lanxin Li. Research on the capacity of charging stations based on queuing theory and energy storage scheduling optimization sharing strategy. *Journal of Energy Storage*, 96:112673, 2024.
- [25] Ting Wu, Emily Fainman, Yasmina Maïzi, Jia Shu, and Yongzhen Li. Allocate electric vehicles’ public charging stations with charging demand uncertainty. *Transportation Research Part D: Transport and Environment*, 130:104178, 2024.
- [26] Huimiao Chen, Hongcai Zhang, Zechun Hu, Yunyi Liang, Haocheng Luo, and Yinhai Wang. Plug-in electric vehicle charging congestion analysis using taxi travel data in the central area of beijing. *arXiv preprint arXiv:1712.07300*, 2017.
- [27] Dan Xiao, Shi An, Hua Cai, Jian Wang, and Haiming Cai. An optimization model for electric vehicle charging infrastructure planning considering queuing behavior with finite queue length. *Journal of Energy Storage*, 29:101317, 2020.
- [28] Christa Brelsford, Sarah Tennille, Aaron Myers, Supriya Chinthavali, Varisara Tansakul, Matthew Denman, Mark Coletti, Joshua Grant, Sangkeun Lee, Karl Allen, et al. A dataset of recorded electricity outages by united states county 2014–2022. *Scientific Data*, 11(1):271, 2024.
- [29] Federal Highway Administration. 2020 nextgen nhts national passenger od data. U.S. Department of Transportation, Washington, DC, 2020. Available online.
- [30] Georgia Department of Revenue, Motor Vehicle Division. Drives e-services—county vehicle registration statistics. <https://eservices.drives.ga.gov>, 2025. Accessed 12 Jun 2025.
- [31] Eric Wood, Brennan Borlaug, Matt Moniot, Dong-Yeon DY Lee, Yanbo Ge, Fan Yang, and Zhaocai Liu. The 2030 national charging network: Estimating us light-duty demand for electric vehicle charging infrastructure. Technical report, National Renewable Energy Laboratory (NREL), Golden, CO (United States), 2023.